
FUNCTION-SPACE MCMC FOR BAYESIAN WIDE NEURAL NETWORKS

A PREPRINT

Lucia Pezzetti
ETH AI Center
lucia.pezzetti@inf.ethz.ch

Stefano Favaro
University of Torino
and Collegio Carlo Alberto
stefano.favaro@unito.it

Stefano Pelucchetti
Cogent Labs
spelucchetti@cogent.co.jp

August 27, 2024

ABSTRACT

Bayesian Neural Networks represent a fascinating confluence of deep learning and probabilistic reasoning, offering a compelling framework for understanding uncertainty in complex predictive models. In this paper, we investigate the use of the preconditioned Crank-Nicolson algorithm and its Langevin version to sample from the reparametrised posterior distribution of the weights as the widths of Bayesian Neural Networks grow larger. In addition to being robust in the infinite-dimensional setting, we prove that the acceptance probabilities of the proposed methods approach 1 as the width of the network increases, independently of any stepsize tuning. Moreover, we examine and compare how the mixing speeds of the underdamped Langevin Monte Carlo, the preconditioned Crank-Nicolson and the preconditioned Crank-Nicolson Langevin samplers are influenced by changes in the network width in some real-world cases. Our findings suggest that, in wide Bayesian Neural Networks configurations, the preconditioned Crank-Nicolson method allows for more efficient sampling of the reparametrised posterior distribution, as evidenced by a higher effective sample size and improved diagnostic results compared with the other analysed algorithms.

1 Introduction

Neural Networks (NNs) have become very popular in the recent years, due to the significant results achieved in various artificial intelligence tasks from speech recognition and image classification, to stock market prediction, healthcare and weather forecasting. Despite this widespread applicability and indisputable success, NNs are hindered by intrinsic shortcomings. The large number of parameters that makes NNs powerful function approximations, is also the reason why NNs are prone to overfitting and overconfidence in their predictions. Moreover, the black-box nature of NNs makes interpretability hard. Bayesian Neural Networks (BNNs) address some of these limitations by providing a principled way to incorporate uncertainty into complex predictive models. At its heart lies the framework of Bayesian Inference, specifically, the weights or parameters of the network are considered to be random variables, instead of deterministic quantities, whose prior beliefs are updated as data are gathered according to the Bayesian learning rule [1, 2, 3, 4, 5, 6, 7].

Despite all these promising advantages and some recent progress, mainly under Gaussian initializations of the weights, BNNs have reached far less popularity than NNs, due to higher computational requirements and limited theoretical understanding. One of the major theoretical challenges concerns the comprehension of the parameter-space behavior of BNNs, in spite of the function one. We therefore explore sampling from the posterior distribution of wide BNNs, focusing on understanding its behavior and properties from a parameter-space perspective. In function space, in fact, under Gaussian initializations of the network's weights, the distribution over the functions induced by wide

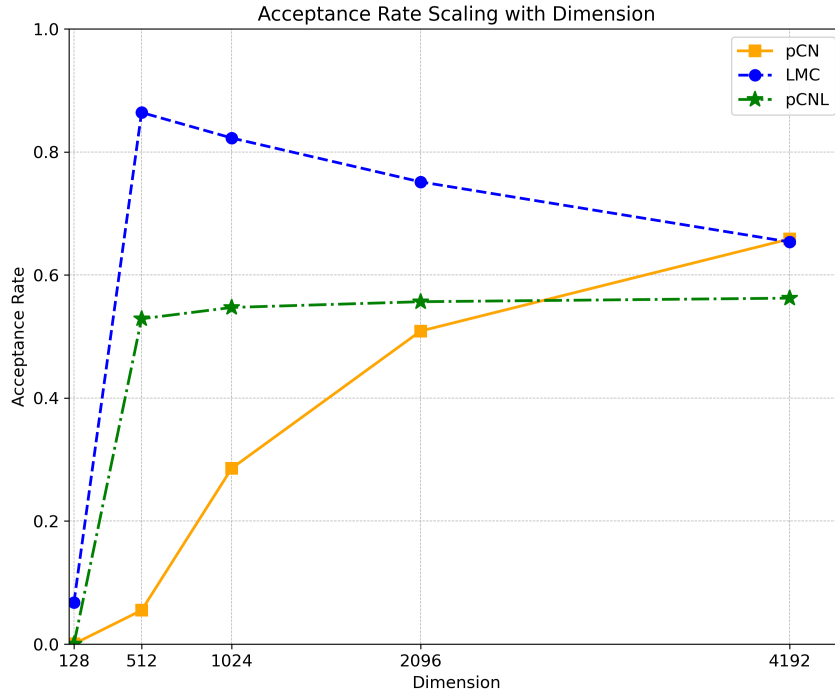


Figure 1: Comparison of the acceptance probability obtained using: i) the underdamped LMC algorithm (or Metropolis Adjusted Langevin Algorithm: MALA); ii) the pCN algorithm; iii) the pCNL method. The neural network architecture used is a fully-connected with one hidden layer, and the layer width varies among the following values: 128, 512, 1024, 2096, 4192. The CIFAR-10 dataset is used, with the sample size fixed at $n = 256$. The stepsize β of the proposal step for all the methods is fixed at 0.1. The acceptance rate of the pCN (orange line) increases steadily as the width of the BNN grows, suggesting improved performance in wide BNNs and highlighting its dimensional independence properties. In contrast, the LMC (blue line) initially shows a rapid acceleration in performance due to the effect of reparametrization. As the width of the network increases, the sampling distribution becomes more similar to an isotropic Gaussian distribution, which makes it better-behaved. However, as the width increases further, the sampler’s non-robustness in high-dimensional settings leads to a progressive deterioration in performance. This confirms the need to decrease the stepsize in order to maintain a constant acceptance rate, which introduces further correlations between the samples. The pCNL method (green line) shows a consistent acceptance rate across all dimensions, indicating a robustness to the dimensional scaling of the BNN. This stability may suggest that the pCNL algorithm effectively combines the strengths of the pCN and LMC methods.

BNNs has been proved to converge to the neural network Gaussian process (NNGP) limit [8, 9, 10, 11, 12, 13, 14]. Recently, [15] provided a counterpart of this result in the parameter space. Specifically, they proved that, after a reparametrization $\phi = T^{-1}(\theta)$ of the flattened NN weights $\theta \in \mathbb{R}^d$, the posterior distribution $p(\phi|\mathcal{D})$ converges in the KL-divergence to the standard Gaussian distribution $\mathcal{N}(0, I_d)$ as the width of the BNN increases. This result not only gives a characterization of the wide-limit parameter distribution, but the closeness to the well-behaved standard normal distribution also suggests that an improvement in the mixing time of Markov chain Monte Carlo (MCMC) sampling procedures is possible. However, standard MCMC procedures are notably non-robust in the infinite-dimensional setting, since their proposal step needs to approach zero for the acceptance rate to remain constant, as the dimension of the space increases.

In this paper, we investigate and provide theoretical guarantees for the use of algorithms that are stable under mesh refinement, namely the preconditioned Crank-Nicolson (pCN) and Crank-Nicolson Langevin (pCNL), to sample from the reparametrised posterior distribution of the weights as the widths of BNNs grow larger. We show that the acceptance probability of both samplers, under reparametrization T , converges to 1 as the width of the BNN layers increases, independently of the chosen fixed stepsize. This result paves the way for a faster and more efficient sampling procedure in wide BNNs. Specifically, not only do the pCN and pCNL proposals avoid suffering from the curse of dimensionality,

but the performance of the samplers intrinsically improves as the BNN becomes larger, without introducing any additional autocorrelation among the samplers. This lessens the need for longer burn-in periods and more samples for adequate convergence diagnostics, which affects standard MCMC methods.

The theoretical guarantees for the use of the pCN and pCNL proposals in wide BNN configurations are empirically supported by a higher effective sample size and improved diagnostic results compared with the LMC algorithm. From a computational point of view, the pCN provides more scalability with respect to derivative-based MCMC algorithms and can scale well to large datasets and complex model. For this reason, the pCN method seems to effectively combine a small computational cost with a significant improvement in the quality of the collected samples, whereas the performance of the pCNL procedure is not striking enough to justify its high computational cost. Notably, improvements in performance increase with the width size but are evident even far from the NNGP regime.

Figure 1 shows the potential of our approach. The acceptance probabilities of the underdamped Langevin Monte Carlo (LMC) [16] the pCN and the pCNL, applied to the posterior of the reparametrized weights, are plotted for a fully-connected network (FCN) with 1 hidden layer. In the samplers a fixed stepsize, $\beta = 0.1$, in the proposal step has been used. As the width of the BNN grows large, the acceptance rate of the pCN algorithm steadily increases, whilst the one of LMC decreases as we go in higher dimension. The pCNL method, instead, shows a consistent acceptance probability across the dimensions. Worth-noting is the initial dramatic increase of the LMC acceptance rate, due to the reparametrization effect that bring the posterior close to the well-behaved standard Gaussian distribution. Further investigations will be provided in Section 4.1.

2 Method

2.1 Notations and preliminaries

Let a dataset $\mathcal{D} = (\mathbf{x}_1, \mathbf{y}_1), \dots, (\mathbf{x}_n, \mathbf{y}_n)$, where $\mathbf{x}_i \in \mathbb{R}^m$ and $\mathbf{y}_i \in \mathbb{R}$. Let parameters θ belong to some parameter space $\Theta \subset \mathbb{R}^D$, for some $D \geq 1$. The prior distribution $p(\theta)$ represents our beliefs prior to observing the data, the beliefs are then updated accordingly to Bayes' rule as data are gathered:

$$p(\theta|\mathcal{D}) = \frac{p(\theta)p(\mathbf{y}|\theta, \mathbf{x})}{p(\mathbf{y}|\mathbf{x})},$$

where $p(\mathbf{y}|\theta, \mathbf{x})$ is the likelihood function.

A BNN is a parametric function $f := f_\theta$ that takes an input \mathbf{x} and produces an output \mathbf{y} . To clarify the notation, we explicitly define the recursion for a fully connected L-hidden layer network with a linear readout layer, i.e.,

$$\begin{aligned} f^{(0)}(\mathbf{x}) &= \frac{\sigma_W^{(1)}}{\sqrt{d^{(0)}}} \mathbf{x} W^{(1)} + \sigma_b^{(1)} \mathbf{1}^{(0)} b^{(1)} \\ g^{(l)}(\mathbf{x}) &= \psi(f^{(l)}(\mathbf{x})), \quad l = 0, \dots, L, \end{aligned} \quad (1)$$

and

$$f^{(l+1)}(\mathbf{x}) = \frac{\sigma_W^{(l+1)}}{\sqrt{d^{(l)}}} g^{(l)}(\mathbf{x}) W^{(l+1)} + \sigma_b^{(l+1)} \mathbf{1}^l b^{(l+1)}, \quad l = 0, \dots, L$$

Thus, $\mathbf{y} = f^{L+1}(\mathbf{x})$ is the output of the network given the input \mathbf{x} . The (non-linear) activation function is denoted by ψ , $d^{(l)}$ denotes the width of the l^{th} layer (with $d^{(0)}$ being the input size m) and $W^{(l)} \in \mathbb{R}^{d^{(l-1)} \times d^{(l)}}$ is its weight matrix. Without loss of generality, in the following we will not make explicit the presence of the bias $b^{(l)} \in \mathbb{R}^{d^{(l)}}$, though we include it in the weight matrix by adding a constant dimension to the outputs of the previous layer so to simplify the notation. The factor $\sigma_W^{l+1}/\sqrt{d^l}$ is to be attributed to the NTK parametrization [17], and it allows to consider an isotropic Gaussian prior for the weights, removing its usual dependence on the width. Precisely, we denote

$$\theta^{(l)} \in \mathbb{R}^{d^{(l)}}, \quad l = 1, \dots, L+1, \quad \theta^{(l)} \sim \mathcal{N}(0, I_{d^{(l)}})$$

the flattened weights of the l^{th} layer, bias included, assumed to be, a priori, independent standard Gaussian random variables. With $\theta \in \mathbb{R}^D$ we consider all the flattened weights $\theta = [\theta^{(l)}]_{l=0, \dots, L} \sim \mathcal{N}(0, I_D)$. We assume a Gaussian likelihood $p(\mathbf{y}|\theta, \mathbf{x}) \sim \mathcal{N}(f^{L+1}(\mathbf{x}), \sigma^2 I_D)$ for the observation variance $\sigma^2 > 0$. Moreover, we assume that $|\psi(x)|$ is bounded by a function of the form $\exp(C\|x\|^{2-\epsilon} - c)$, for some $C, c, \epsilon > 0$; we refer to [12] for similar assumptions on the activation function.

We are interested in theoretical guarantees for sampling from the posterior distribution of the weights as the width grows. [15] proposed the following data-dependent reparametrization of the readout layer weights of BNNs:

$$\phi^{(l)} = \begin{cases} \Sigma^{-1/2} (\theta^{(l)} - \mu) & l = L + 1 \\ \theta^{(l)} & \text{otherwise} \end{cases} \quad (2)$$

where, defining $\Psi = \frac{\sigma_W^{(L+1)}}{\sqrt{d^{(L)}}} g^{(L)}(\mathbf{x})$, we have

$$\Sigma = (I_{d^L} + \sigma^{-2} \Psi^T \Psi)^{-1}, \quad \mu = \sigma^{-2} \Sigma \Psi^T y. \quad (3)$$

The reparametrized posterior distribution, whose density function is denoted by $p(\phi|\mathcal{D})$, is shown to converge in the KL-divergence to a standard Gaussian $\mathcal{N}(0, I_D)$ as the width goes to infinity. In particular, the convergence to a simple isotropic Gaussian suggests potential improvements in the mixing speed of MCMC procedures, compared to sampling from the notably arduous BNN posterior. Nevertheless, standard MCMC algorithms, such as the Random Walk Metropolis-Hastings Algorithm (RW-MH) and the Metropolis Adjusted Langevin Algorithm (LMC), are notoriously ill-suited for the infinite-dimensional setting and must be carefully re-tuned as the dimension increases to avoid degeneracy in the acceptance probability. Indeed, the optimal scaling properties of the RW-MH and LMC algorithms have been derived in [18] and [19], respectively. There, it is shown that the proposal movements need to vanish as the dimension of the parameter space grows unbounded for factorial target distributions. Consequently, the efficiency of the RW-MH and LMC algorithms vanishes as well.

2.2 Function-Space MCMC

Since our interest lies in analyzing the behavior of wide networks, we need methods that are robust in the infinite dimensional setting. A class of such MCMC algorithms have been early derived and discussed in [20]. In this section, we focus on the pCN and pCNL methods and briefly contrast them with their traditional counterparts: the RW-MH and the LMC algorithms. The slight modifications introduced in pCN and pCNL made them robust and well-defined in high dimensional settings, contrasting the well known degeneracy of the standard MCMC acceptance probability as the dimension increases.

RH-MC employs a symmetric proposal, typically Gaussian, centered at the current state to explore the parameter space, i.e.,

$$v = u + \beta w, \quad w \sim \mathcal{N}(0, \mathcal{C}), \quad \beta \in (0, 1]$$

Instead, the pCN algorithm relies on the following modification of the (standard) random walk proposal:

$$v = \sqrt{1 - \beta^2} u + \beta w, \quad w \sim \mathcal{N}(0, \mathcal{C}), \quad \beta \in (0, 1] \quad (4)$$

where \mathcal{C} is the covariance operator of the prior Gaussian measure. See [20] and references therein for details on RH-MC and pCN proposals.

The pCN algorithm is reversible with respect to an arbitrary Gaussian measure, and hence admits such Gaussian measure as invariant distribution. Specifically, in our context, we set the invariant Gaussian measure to be equal to an isotropic Gaussian distribution (the prior). The acceptance probability reduces to:

$$a(v|u) = \min\{1, \exp(-\ell(u) + \ell(v))\}. \quad (5)$$

where ℓ is the log-likelihood. The steps of the pCN procedures are listed in Algorithm 1.

Despite being agnostic about which parts of the state space are more probable, the pCN proposal is, by construction, well-defined in the infinite-dimensional setting. This motivated us to study the procedure to sample from the above reparametrized weights posterior distribution. In our context, the proposal 4 is

$$\phi^* = \sqrt{1 - \beta^2} \phi + \beta w \quad w \sim \mathcal{N}(0, I_D) \implies q(\phi^*|\phi) = \mathcal{N}(\sqrt{1 - \beta^2} \phi, \beta^2 I_D),$$

where $\beta \in [0, 1)$. Now, by including this expression in the acceptance probability 5, we can prove the following theorem.

Theorem 2.1 *Consider the BNN model with the reparametrisation 2. Then, the acceptance probability of the pCN algorithm to sample from the reparametrised weight posterior, for any $\beta \in [0, 1)$, converges to 1 as the width of the network increases. If d_{min} is the smallest among the network's layer widths, then*

$$a(\phi^*|\phi) = \min \left\{ 1, \frac{p(\phi^*|\mathcal{D})q(\phi|\phi^*)}{p(\phi|\mathcal{D})q(\phi^*|\phi)} \right\} \rightarrow 1 \quad \text{as } d_{min} \rightarrow \infty$$

Algorithm 1 Preconditioned Crank-Nicolson (pCN) Algorithm

```

1: Initialize  $u^{(0)}$ , set number of iterations  $N$ , choose  $\beta \in (0, 1]$ 
2: for  $n = 0$  to  $N - 1$  do
3:   Propose  $v = \sqrt{1 - \beta^2}u^{(n)} + \beta N(0, C)$ 
4:   Calculate acceptance probability  $a(v|u^{(n)}) = \min\{1, \exp(-\ell(u^{(n)}) + \ell(v))\}$ 
5:   Draw  $\eta \sim \text{Uniform}(0, 1)$ 
6:   if  $\eta \leq a(v|u^{(n)})$  then
7:     Set  $u^{(n+1)} = v$ 
8:   else
9:     Set  $u^{(n+1)} = u^{(n)}$ 
10:  end if
11: end for

```

See Appendix A for the proof of Theorem 2.1.

The MALA algorithm incorporates gradient information from the log-posterior distribution in the proposal mechanism to guide the sampling process. More precisely, this method involves simulating Langevin diffusion such that the solution to the time evolution equation is a stationary distribution that equals the target density (in Bayesian contexts, the posterior distribution). This approach is particularly effective in exploring complex, high-dimensional probability distributions by making proposals that are more informed and therefore likely to be accepted. The mathematical expression of the proposal is:

$$v = u + \frac{\epsilon^2}{2} \nabla \log p(u|D) + \epsilon w, \quad w \sim N(0, I)$$

where v is the current position of the algorithm in the parameter space, and ϵ is the step size, which is a tuning parameter that allows to control the scale of the updates. In particular, $\nabla \log p(\phi|D)$ is the gradient of the log-posterior density, which provides the direction towards higher probability densities.

While MALA provides an efficient way to explore the parameter space, it can still struggle in scenarios where the parameter space is high-dimensional. This led to the development of the pCNL algorithm, which introduces little modifications to better handle these challenges. Its proposal is derived by discretization of a stochastic partial differential equation (SPDE) which is invariant for target measure and is given by:

$$v = \frac{1}{2 + \delta} \left[(2 - \delta)u + 2\delta \mathcal{C} \mathcal{D} \ell(u) + \sqrt{8\delta} w \right], \quad w \sim \mathcal{N}(0, \mathcal{C}), \quad \delta \in (0, 2) \quad (6)$$

where \mathcal{C} is the covariance operator of the Gaussian prior measure, ℓ is the log-likelihood, and $\mathcal{D} \ell$ denotes its Fréchet derivative. Note that the parameter δ is directly related to the pCN stepsize β by the relationship $\beta^2 = 8\delta / (2 + \delta)^2$. Throughout the paper, we refer to the stepsize as β , and we keep into account this relationship when dealing with the pCNL proposal. When the pCNL is used as a proposal for a MH scheme, the acceptance probability is given by

$$a(v|u) = \min\{1, \exp(\rho(u, v)) - \rho(v, u)\} \quad (7)$$

, where

$$\rho(u, v) = -\ell(u) - \frac{1}{2} \langle v - u, \mathcal{D} \ell(u) \rangle - \frac{\delta}{4} \langle u + v, \mathcal{D} \ell(u) \rangle + \frac{\delta}{4} \|\sqrt{\mathcal{C}} \mathcal{D} \ell(u)\|^2$$

These modifications ensure that pCNL retains the efficiency of MALA in terms of informed proposals while enhancing its applicability and robustness in more challenging high-dimensional settings. The steps of the pCNL procedures are presented in Algorithm 2.

It is therefore natural to ask whether also the acceptance probability of the pCNL algorithm converges to one as the network width increases.

Firstly recall the pCNL proposal 6 that, using the notation introduced with the reparametrisation 2, can be written as:

$$\phi^* = \frac{1}{2 + \delta} \left[(2 - \delta)\phi + 2\delta \mathcal{C} \mathcal{D} \ell(\phi) + \sqrt{8\delta} Z \right], \quad Z \sim \mathcal{N}(0, \mathcal{C})$$

where $\delta \in (0, 2)$.

Algorithm 2 Preconditioned Crank-Nicolson Langevin (pCNL) Algorithm

```

1: Initialize  $u^{(0)}$ , set number of iterations  $N$ , choose  $\delta \in (0, 2)$ 
2: for  $n = 0$  to  $N - 1$  do
3:   Propose  $v = \frac{1}{2+\delta} \left[ (2 - \delta)u^{(n)} + 2\delta\mathcal{C}\mathcal{D}\ell(u^{(n)}) + \sqrt{8\delta}\mathcal{N}(0, \mathcal{C}) \right]$ 
4:   Calculate acceptance probability  $a(v|u^{(n)}) = \min \left\{ 1, \frac{p(v|\mathcal{D})}{p(u^{(n)}|\mathcal{D})} \right\}$ 
5:   Draw  $\eta \sim \text{Uniform}(0, 1)$ 
6:   if  $\eta \leq a(v|u^{(n)})$  then
7:     Set  $u^{(n+1)} = v$ 
8:   else
9:     Set  $u^{(n+1)} = u^{(n)}$ 
10:  end if
11: end for

```

Then, when the pCNL proposal is applied in the MH procedure, the acceptance probability 7 assumes the following expression:

$$acc_{pCNL} = \min \{1, \exp(\rho(\phi, \phi^*) - \rho(\phi^*, \phi))\}$$

where

$$\rho(\phi, \phi^*) = -\ell(\phi) - \frac{1}{2}\langle \phi^* - \phi, \mathcal{D}\ell(\phi) \rangle - \frac{\delta}{4}\langle \phi + \phi^*, \mathcal{D}\ell(\phi) \rangle + \frac{\delta}{4}\|\sqrt{\mathcal{C}}\mathcal{D}\ell(\phi)\|^2$$

and, in our case, $\mathcal{C} = I$.

The following theorem provides the convergence of the acceptance probability of the pCNL algorithm to one as the network width increases.

Theorem 2.2 *Consider the BNN model with the reparametrisation 2. Then, the acceptance probability of the pCNL algorithm to sample from the reparametrised weight posterior, for any $\delta \in (0, 2)$, converges to 1 as the width of the network increases. That is to say, if d_{min} is the smallest among the network's layer widths, then*

$$a(\phi^*|\phi) = \min \left\{ 1, \frac{p(\phi^*|\mathcal{D})q(\phi|\phi^*)}{p(\phi|\mathcal{D})q(\phi^*|\phi)} \right\} \rightarrow 1 \quad \text{as } d_{min} \rightarrow \infty$$

See Appendix B for the proof of Theorem 2.2.

3 Marginal-Conditional Decomposition

An alternative approach to Theorem 2.1 involves marginalizing the weights of the network's final layer and perform the sampling procedure only on the weights of the network's inner layers. This idea is effective since it acknowledges that exact sampling can be performed from the posterior distribution of the reparametrized weights of the last layer, once the weights from all preceding layers are known, i.e.,

$$\begin{aligned} p(\phi|\mathcal{D}) &= p(\phi^{(L+1)}|\phi^{(\leq L)}, \mathcal{D})p(\phi^{(\leq L)}|\mathcal{D}) \\ &= p(\phi^{(L+1)}|\theta^{(\leq L)}, \mathcal{D})p(\theta^{(\leq L)}|\mathcal{D}) \end{aligned}$$

where the last equality follows directly from the reparametrisation definition and from the fact that $p(\phi^{(L+1)}|\theta^{(\leq L)}, \mathcal{D}) \sim \mathcal{N}(0, I_{d^{(L)}})$ for any fixed value of $\theta^{(\leq L)}$. The idea is then to simply perform pCN sampling on the posterior distribution over the inner-layers weights $\pi(\theta^{(\leq L)}|\mathcal{D})$. Then, once the samples

$$\left[\theta_i^{(\leq L)} \right]_{i=1, \dots, n}$$

have been collected, we draw, $\forall i, \phi_i^{(L+1)} \sim \mathcal{N}(0, I_{d^{(L)}})$, to obtain a sample of the full posterior distribution of the reparametrised weights. On the pCN algorithm, the next theorem is a counterpart of Theorem 2.1:

Theorem 3.1 *Consider the BNN model with the reparametrisation 2, and set $p(\theta|\mathcal{D}) = p(\phi^{(L+1)}|\theta^{(\leq L)}, \mathcal{D})p(\theta^{(\leq L)}|\mathcal{D})$ and $\theta^{(\leq L)} = W$. Then, the acceptance probability of the pCN algorithm, for any $\beta \in [0, 1)$, applied to $p(\theta^{(\leq L)}|\mathcal{D})$*

converges to 1 as the width of the network increases. If d_{min} is the smallest among the network’s layer widths, then

$$a(\phi^*|\phi) = \min \left\{ 1, \frac{p(W^*|\mathcal{D})q(W|W^*)}{p(\phi|\mathcal{D})q(W^*|W)} \right\} \rightarrow 1 \quad \text{as } d_{min} \rightarrow \infty$$

See Appendix C for the proof of Theorem 3.1.

4 Numerical Experiments

We test our framework to validate the theory and highlight its applicability. In the setting of Theorems 2.1 and 2.2, we compare the performance of the pCN algorithm, the underdamped LMC sampler and the pCNL methods on the reparametrized posterior of a fully connected feed-forward BNN. We replicate the setting used by [15]: the CIFAR-10 dataset, with one-hot encoding and $-1/10$ label shifting, is used in all the experiments, the likelihood is Gaussian with a fixed standard deviation of $\sigma = 0.1$ and sample thinning is consistently applied. A fair comparison between the different samplers is achieved by equalizing their stepsize β , that in our context always refers to the coefficient multiplying the noise in the proposal step. The code is available at github.com/lucia-pezzetti/Function-Space-MCMC-for-Wide-BNNs.

4.1 Acceptance Rate Convergence

The first result we report in Figure 2 is the numerical illustration of the behavior of the pCN, LMC and pCNL acceptance rates as the width of the BNN grows large. To be more precise, the acceptance probabilities of the underdamped LMC the pCN and the pCNL, applied to the posterior of the reparametrized weights, are plotted for a FCN with 1 hidden layer. For each subplot a fixed stepsize, respectively $\beta = 0.2$, $\beta = 0.1$ and $\beta = 0.01$, has been used in the proposal step. The figure clearly displays that, for all stepsizes, the acceptance rate of the pCN algorithm steadily increases with the layer width, empirically showcasing the theoretical result presented in Theorem 2.1. Even if its acceptance rate increases as the width grows, as expected from what we will demonstrate in Theorem 2.2, the convergence rate seems to be heavily affected by the stepsize. Indeed, for the largest stepsize, $\beta = 0.2$, the trend is quite evident, whereas for the other two stepsizes the acceptance rate increases only marginally when the number of hidden units vary from 512 to 4192 and appears almost constant. A possible explanation for this unexpected findings can lie in the fact that the convergence of the pCNL acceptance rate is more elaborated than the pCN one, as clear from the Proof B and this may lead to unpredicted consequences in its empirical results. Finally, the profile of the LMC acceptance rates confirm and reflect the reason why we started our investigations: the MCMC methods’ non-robustness in high-dimensional settings leads to a progressive decline of its acceptance rate as the width increases that should be compensated by decreasing the method stepsize.

We then proceed by analyzing the quality of the samplers using two key diagnostic tools: the effective sample size and the Gelman-Rubin statistic.

4.2 Diagnostic: Effective Sample Size

We assess the performance of the MCMC using the effective sample size (ESS). In particular, for an MCMC-based estimator, the ESS estimates the number of independent samples that are equivalent, in terms of their standard variance, to the correlated Markov chain samples collected. In practical implementations, we use TensorFlow Probability’s built-in function, `tfp.mcmc.effective_sample_size`, to compute the ESS [21].:

$$ESS(N) = \frac{N}{1 + 2 \sum_{i=1}^{N-1} (1 - \frac{i}{N}) R_i},$$

where the resulting sequence of auto-correlations is truncated after the first appearance of a term that is less than zero. In particular, the per-step ESS will be calculated by dividing the above expression by N .

4.3 Diagnostic: Gelman-Rubin Statistic

The Gelman-Rubin statistic or potential scale reduction factor, \hat{R} , [22, 23] complements the ESS analysis by assessing how the different samples affect the rate of convergence of the collected Markov chain. More precisely, the metric is evaluated by running multiple independent chains per each sample and then exploiting comparisons of the variance between multiple chains to the variances within the single chains to give a measure of the degree to which variance (of the means) between chains exceeds what one would expect if the chains were identically distributed. Mathematically,

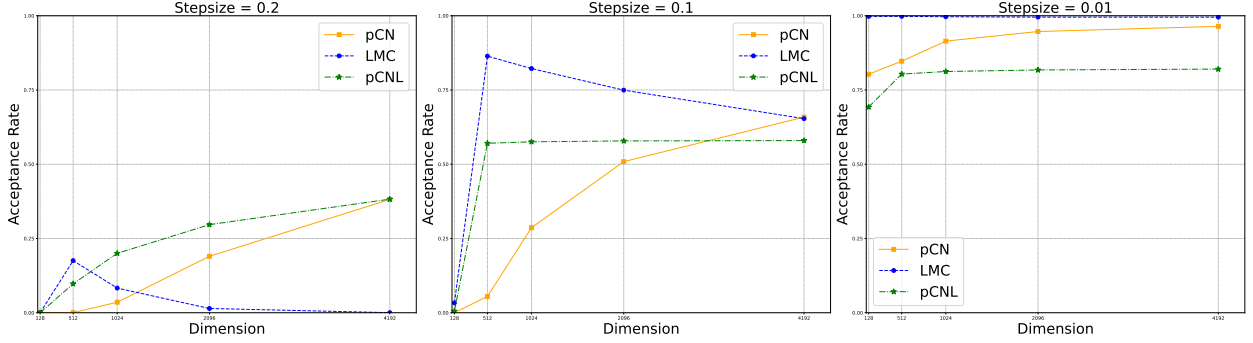


Figure 2: Comparison at different stepsizes ($\beta = 0.2, 0.1, 0.01$) of the acceptance probability obtained using: i. the underdamped LMC algorithm (or Metropolis Adjusted Langevin Algorithm: MALA); ii. the pCN algorithm; iii. the pCNL method. The neural network architecture used is a fully-connected with one hidden layer, and layer width that varies among the following values: 128, 512, 1024, 2096, 4192. The CIFAR-10 dataset is used, with the sample size fixed at $n = 256$. The acceptance rate of the pCN (orange line) increases steadily as the width of the BNN grows at every stepsize, suggesting improved performance in wide BNNs, highlighting its robustness in high-dimensional settings and empirically confirming our theoretical analysis. In contrast, the LMC (blue line) initially shows a rapid acceleration in performance due to the reparametrization effect, indeed as the width of the network increases, the sampling distribution becomes more similar to an isotropic Gaussian distribution, which makes it better-behaved and the sampling procedure more effective. However, as the width increases further, the sampler’s non-robustness in high-dimensional settings leads to a progressive decline of its acceptance rate. This confirms the need, in standard MCMC procedures, to carefully decrease the stepsize in order to maintain a constant acceptance rate, which, inevitably, introduces further correlations between the samples. This behavior is less visible, but slightly present, also for the smallest stepsize, $\beta = 0.01$ for which the LMC acceptance rate remains constantly over 0.99. Finally, the pCNL acceptance rate (green line) exhibits a slower progress toward 1 as the width increases, compared to the pCN, and the rate seems to be also heavily dependent on the stepsize. Indeed, whereas the convergence is quite evident for $\beta = 0.2$, for both the other stepsizes the acceptance rate increases only marginally as the width grows and appear as almost constant.

the Gelman-Rubin statistic is defined as follows: Suppose we have run M chains in parallel with different starting values and that we have collected N samples for each chain. Denote by $x_i^{(m)}$ the i -th sample of the m -th chain. The within-chain variance and the between-chain variance are defined as:

$$W = \frac{1}{M} \sum_{m=1}^M s_m^2, \quad B = \frac{N}{M-1} \sum_{m=1}^M (\bar{x}^{(\cdot)} - \bar{x}^{(m)})^2,$$

where s_m^2 is the sample variance of the m -th chain, $\bar{x}^{(m)}$ its mean and $\bar{x}^{(\cdot)}$ is the grand mean. The Gelman-Rubin statistic is then defined as:

$$\hat{R} = \frac{\frac{N-1}{N}W + \frac{1}{N}B}{W}.$$

Now, since at convergence all the parallel chains are indistinguishable, the Gelman-Rubin statistic should be close to 1. In practice, a value of \hat{R} smaller than 1.2 is considered as a good indicator of approximate convergence [22].

In all the following experiments we make use of the TensorFlow Probability’s built-in function, `tfp.mcmc.potential_scale_reduction`, to compute \hat{R} .

4.4 Real World Application

We examine and compare how the efficiency of the LMC, the pCN and the pCNL samplers are influenced by changes in network width, using per-step ESS as the performance metric. Our analysis was conducted using a single chain over one million steps, excluding the first 20,000 steps as burn-in for each configuration tested, and we thin by collecting every 25th step from the chain. In all experiments, we used a single-layer, fully connected feed-forward neural network with GELU activation functions [24]. We adhered to the weight and bias scaling described in Section 1.1 of [15], setting the scaling factors to $\sigma_W^2 = 2$ and $\sigma_b^2 = 0.01$ across all layers except for the output layer, where σ_W^2 was set to 1 to maintain unit variance of the network’s initial predictions under the prior distribution.

In this setting, we focused on evaluating the samplers’ performance as the network width increased, seeking empirical validation of our theory. We fixed the dataset size at $n=256$ and allowed the network width to range from 128 to 4192, increasing according to powers of 2. Reparametrization 2 was used for all samplers.

Empirical findings are shown in Figure 3, which compares the efficiency of the samplers using the per-step ESS metric across various widths. Specifically, the solid lines represent the average ESS per step for each width, while the shaded regions indicate the minimum and maximum values over the whole run. The reported plots correspond to the stepsizes $\beta = 0.2$ (above), $\beta = 0.1$ (in the middle) and $\beta = 0.01$ (below).

We analyze the plots for the three stepsizes separately before giving a general overview of the results. For $\beta = 0.2$, the LMC sampler exhibits an extremely low per-step ESS across all widths, reflecting its suboptimal acceptance rate. In particular, the metric seems to reach zero with almost no variability for the larger widths. The pCN sampler, on the other hand, is characterized by a steady increase in its per-step ESS, underlining how the increase in acceptance rate actually helps to boost the performance and the efficiency of the sampler. Indeed, the rise in the acceptance rate for a constant stepsize does not introduce further correlation among the samples, but rather allows the sampler to explore the space more effectively. The pCNL, as we expected from the theoretical analysis, behaves similarly to the pCN, although the increase in the ESS is less pronounced. Moreover, the pCNL maintains the highest per-step ESS in all but the largest dimension, where the pCN eventually reaches it. This, together with the fact that the pCNL is computationally more demanding than the pCN, starts to suggest that it may be a less attractive option for wide BNNs.

For $\beta = 0.1$, the performances of LMC and pCN described for the previous stepsize are even more accentuated. The LMC procedure is characterized by an initial significant rise in per-step ESS as the network width increases, that can be attributed to the reparametrization effect: the sampling distribution becomes more similar to an isotropic Gaussian leading to an increase in the performance of the sampler and in the acceptance rate. However, as the width increases further, the well-known MCMC methods’ non-robustness in high-dimensional settings leads to a progressive deterioration in performance, thus confirming the need to carefully decrease the stepsize for the efficacy to not diminish. The pCN proposal, instead, is still associated to a dramatic increase in the ESS as the network width grows and the same analysis as before can be applied. Worth-noting is that, as expected, bigger stepsizes introduce less autocorrelation among the collected data points and hence lead to higher ESS values. Finally, the pCNL method shows a more stable performance, with even an unexpected slight decline in the ESS as the width becomes larger. This may be justified by the fact that the convergence of the pCNL acceptance rate depends on more factors than the pCN one, this may lead to unpredicted consequences in its empirical results. Nevertheless, the pCNL maintains the highest per-step ESS in all widths but the largest one.

For the smallest stepsize, $\beta = 0.01$, the outcomes of the simulations are rather different. Both the pCN and the pCNL algorithms exhibit a strong autocorrelation among the samples, due to the too small stepsize and the construction itself of the proposals. This leads to an extremely low per-step ESS despite the high acceptance rate. The LMC method, conversely and surprisingly, shows significant values of per-step ESS, even if decreasing as the network width increases. This is particularly striking if these values are compared to the ones obtained for $\beta = 0.1$, for which the LMC’s acceptance rate was closer to the suggested optimal one [19]. Despite this unexpected behavior, the efficacy of the sampling procedure is still declining as the dimension grows and, since the acceptance rate remains almost constant, maintaining it stable doesn’t seem an easy task to achieve.

In general, the results of the experiments are consistent with the theoretical analysis. The pCN sampler, in particular, emerges as the most appropriate method for sampling from the reparametrized posterior of wide BNNs. Nevertheless, it is crucial to not set the stepsize too small, as this would lead to a significant increase in the autocorrelation among the samples and a consequent decrease in the ESS. At lower widths, instead, tuning the stepsize of the LMC method to reach an acceptance rate over 98% is the option that guarantees the best results. Finally, the pCNL method seems not to have meaningful enough outcomes to justify its use in this context, especially if we take into account its heavy computational demands.

We now shift our focus to the Gelman-Rubin statistic in order to assess the convergence of Markov chains to the target distribution. We examine the \hat{R} values for the pCN, LMC, and pCNL samplers, considering their evolution as a function of the number of steps [5000, 10000, 15000, 20000]. The stepsize is fixed at $\beta = 0.1$. For each sampler, we run three independent chains for each of the BNN widths among $\{512, 1024, 2096, 4192\}$, we then use the collected samples to calculate the metric values. More specifically, our focus is on investigating how the \hat{R} values for different widths of the BNN change as the number of steps increases for the different samplers. This analysis allows us to evaluate and compare the convergence efficiency of the different samplers across these varying network sizes. The results are presented in Figure 4, where we also plot the reference line of $\hat{R} = 1.2$ to indicate the standard empirical threshold for determining convergence.

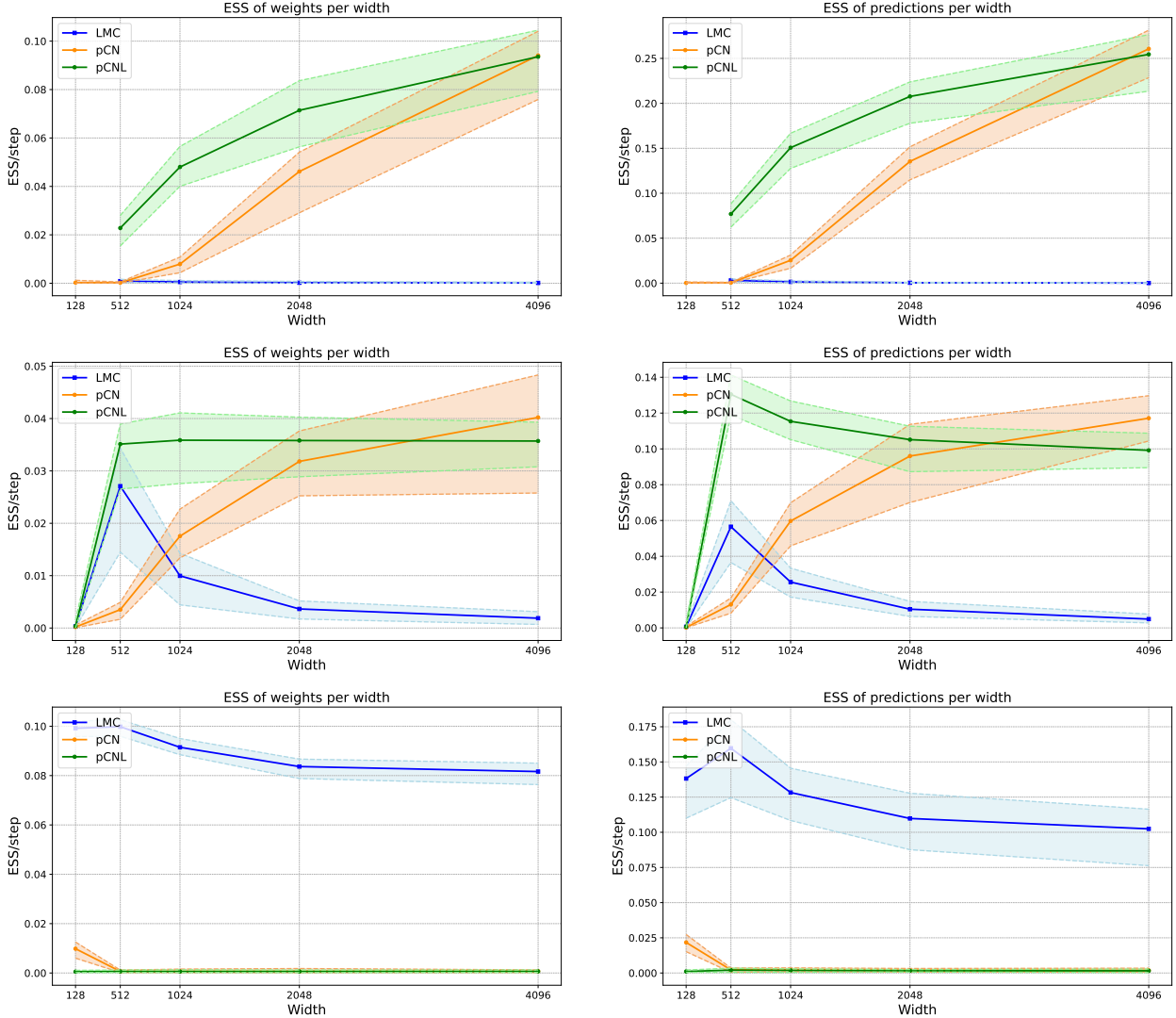


Figure 3: ESS analysis of the LMC, pCN and pCNL algorithms as a function of the 1-layer FCN’s width for stepsizes $\beta = 0.2$ (above), $\beta = 0.1$ (middle) and $\beta = 0.01$ (below). The solid lines represent the average per-step ESS, whereas the shaded areas indicate the variability of the per-step ESS delineated by its minimum and maximum values. The setting used in the experiments is the same as the setting of Figure 2: the layer width of the BNN varies among the following values: $\{128, 512, 1024, 2096, 4192\}$. The CIFAR-10 dataset is used, with sample size fixed at $n = 256$. Beginning with the highest stepsize, $\beta = 0.2$, the LMC performance is very poor among all dimensions due to the suboptimal acceptance probability. The pCN sampler, instead, shows a constant growth in ESS as the network width increases, indicating that enhancements in acceptance rate contribute positively to efficiency and performance. The pCNL approach shows a similar but less pronounced behavior, maintaining the highest per-step ESS in all but the largest dimensions where pCN eventually reaches it. For $\beta = 0.1$, the LMC method initially demonstrates a significant rise in ESS as the network width increases, reflecting the increase in acceptance rate due to reparametrization. However, its effectiveness sharply decreases in higher-dimensional settings due to its inherent limitations. pCNL displays a more stable performance, although the ESS slightly decreases with increasing dimensionality. Conversely, pCN consistently demonstrates significant improvements in ESS, reaffirming its robustness in larger BNN architectures. Finally, the smallest stepsize, $\beta = 0.01$ heavily affects the behavior of both the pCN and the pCNL samplers which exhibit strong autocorrelation among the samplers. Instead, while LMC’s ESS decreases, it remains relatively robust across all dimensions. This underscores the distinction between proving an acceptance probability approaching unity for every fixed stepsize and achieving such a probability through stepsize reduction. Smaller stepsizes inevitably lead to higher correlations, reduced ESS, and diminished performance. Maintaining a larger stepsize is beneficial as it avoids introducing additional correlations.

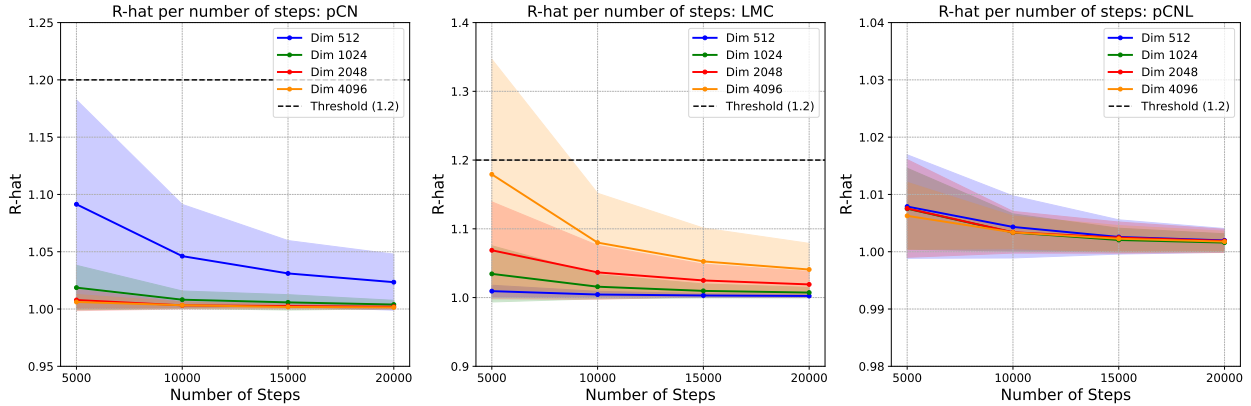


Figure 4: Evolution of the Gelman-Rubin statistic, evaluated using three independent chains, of the LMC, pCN and pCNL as a function of the number of steps for the stepsize $\beta = 0.1$. The solid lines represent the average Gelman-Rubin statistic, whereas the shaded areas indicate their standard deviation. Again, the CIFAR-10 dataset, with sample size fixed at $n = 256$, is used. Since the metric should be close to 1 for all chains to be considered converged, we trace a horizontal line at $\hat{R} = 1.2$, indicating the standard empirical threshold for determining convergence. For all samples the chosen burn-in of 20,000 steps appears to be sufficient to ensure that the chains have reached the target distribution. However, we can still notice some peculiarities. The metric for pCN sampler improves as the width increases, convalidating even more the robustness of the method in high-dimensional settings. The LMC method shows complementary results, with an increase in the Gelman-Rubin statistic as the network width grows. Finally, the pCNL approach exhibits extraordinary good results among all the dimensions.

In the first place we observe that for all samplers the chosen burn-in of 20,000 steps appears to be adequate to ensure that the chains have reached stationarity. Nevertheless, the samplers present some peculiarities that are worth to discuss. The pCN sampler, shows a less variable and closer to 1 Gelman-Rubin statistic as the network width increases, suggesting that the chain attains stationarity quicker and more steadily for large network widths. This is in line with the previously obtained results and confirms once again pCN suitability in wide BNNs settings. Not surprisingly, the LMC results seems the negative version of the pCN ones. Indeed, its \hat{R} values reflects the better performance of the sampler in lower dimensions, as underlined by its increase in both the average and standard deviation as the width grows. Finally, the pCNL procedure exhibits exceptionally good results among all dimensions, with the \hat{R} values that are always close to 1 and have small variability. This is a very interesting result, since it highlights the ability of the sample to properly explore the space and quickly approach the target distribution.

5 Conclusion

In this paper, we investigated the effectiveness of the pCN and pCNL samplers in sampling wide Bayesian Neural Networks (BNNs), and we provided insights into the scalability and efficiency of these methods; particularly when compared to the underdamped LMC sampler. Our theoretical findings, grounded in the understanding of the reparameterized posterior distribution, demonstrated that the acceptance probability of the pCN proposal converges to 1 as the network width goes to infinity, thus ensuring efficient sampling. Empirical results further corroborated this theoretical prediction. When applied to fully connected networks with varying widths, pCN consistently demonstrated higher per-step ESS compared to LMC, especially as dimensionality increased. This finding is crucial as it underscores the advantage of the pCN approach in wide Bayesian neural networks, where standard MCMC techniques often struggle due to high autocorrelation among samples. Our results indicate that the pCN sampler, under the proposed framework, offers a reliable and scalable solution for Bayesian inference in wide neural networks, ultimately leading to better diagnostic performance and improved computational efficiency. The dimensional robustness of the pCNL method, along with the incorporation of gradient information within the MH proposal, makes it effective and stable for posterior sampling from BNNs. However, the method is significantly more expensive computationally compared to pCN and therefore, given the absence of significant increases in performance as the network width grows larger, the pCN version is preferred in very large width regimes.

Limitations

Due to constraints in our computational resources, we were not able to run experiments on BNNs with wider layers. However, based on our current analyses, as presented in the acceptance probability analysis of Figure 2 and in the ESS analysis of Figure 3, we anticipate a widening performance gap between the LMC and pCN samplers with increased layer width. Theoretically, we showed that the acceptance rates for pCN and pCNL converge to 1, supporting the scalability and robustness of the algorithms. In contrast, the LMC sampler’s acceptance rate is known to decrease further as layer width increases. This anticipated behavior suggests an increase in autocorrelation among samples from the LMC, and a decrease in autocorrelation for the pCN samples. These projections underscore the potential limitations of LMC samplers in handling larger BNNs, highlighting the need for more robust sampling methods in extensive computational settings. Finally, it would be interesting to extend these empirical analyses to other neural network architectures and to deep neural networks.

References

- [1] Mohammad Emtiyaz Khan and Didrik Nielsen and Voot Tangkaratt and Wu Lin and Yarin Gal and Akash Srivastava. Fast and Scalable Bayesian Deep Learning by Weight-Perturbation in Adam. *arXiv preprint arXiv:1806.04854*, 2018.
- [2] Wesley Maddox and Timur Garipov and Pavel Izmailov and Dmitry Vetrov and Andrew Gordon Wilson. A Simple Baseline for Bayesian Uncertainty in Deep Learning. *arXiv preprint arXiv:1902.02476*, 2019.
- [3] Kazuki Osawa and Siddharth Swaroop and Anirudh Jain and Runa Eschenhagen and Richard E. Turner and Rio Yokota and Mohammad Emtiyaz Khan. Practical Deep Learning with Bayesian Principles. *arXiv preprint arXiv:1906.02506*, 2019.
- [4] Michael W. Dusenberry and Ghassen Jerfel and Yeming Wen and Yi-An Ma and Jasper Snoek and Katherine Heller and Balaji Lakshminarayanan and Dustin Tran. Efficient and Scalable Bayesian Neural Nets with Rank-1 Factors. *arXiv preprint arXiv:2005.07186*, 2020.
- [5] Erik Daxberger and Eric Nalisnick and James Urquhart Allingham and Javier Antorán and José Miguel Hernández-Lobato. Bayesian Deep Learning via Subnetwork Inference. *arXiv preprint arXiv:2010.14689*, 2022.
- [6] Pavel Izmailov and Sharad Vikram and Matthew D. Hoffman and Andrew Gordon Wilson. What Are Bayesian Neural Network Posteriors Really Like? *arXiv preprint arXiv:2104.14421*, 2021.
- [7] Radford M. Neal. Bayesian Learning for Neural Networks. Springer-Verlag, Berlin, Heidelberg, 1996.
- [8] Alexander G. de G. Matthews and Mark Rowland and Jiri Hron and Richard E. Turner and Zoubin Ghahramani. Gaussian Process Behaviour in Wide Deep Neural Networks. *arXiv preprint arXiv:1804.11271*, 2018.
- [9] Jaehoon Lee and Yasaman Bahri and Roman Novak and Samuel S. Schoenholz and Jeffrey Pennington and Jascha Sohl-Dickstein. Deep Neural Networks as Gaussian Processes. *arXiv preprint arXiv:1711.00165*, 2018.
- [10] Roman Novak and Lechao Xiao and Jaehoon Lee and Yasaman Bahri and Greg Yang and Jiri Hron and Daniel A. Abolafia and Jeffrey Pennington and Jascha Sohl-Dickstein. Bayesian Deep Convolutional Networks with Many Channels are Gaussian Processes. *arXiv preprint arXiv:1810.05148*, 2020.
- [11] Adrià Garriga-Alonso and Carl Edward Rasmussen and Laurence Aitchison. Deep Convolutional Networks as shallow Gaussian Processes. *arXiv preprint arXiv:1808.05587*, 2019.
- [12] Greg Yang. Tensor Programs I: Wide Feedforward or Recurrent Neural Networks of Any Architecture are Gaussian Processes. *arXiv preprint arXiv:1910.12478*, 2021.
- [13] Jiri Hron and Yasaman Bahri and Roman Novak and Jeffrey Pennington and Jascha Sohl-Dickstein. Exact posterior distributions of wide Bayesian neural networks. *arXiv preprint arXiv:2006.10541*, 2020.
- [14] Daniele Bracale and Stefano Favaro and Sandra Fortini and Stefano Peluchetti. Large-width functional asymptotics for deep Gaussian neural networks. *arXiv preprint arXiv:2102.10307*, 2021.
- [15] Jiri Hron and Roman Novak and Jeffrey Pennington and Jascha Sohl-Dickstein. Wide Bayesian neural networks have a simple weight posterior: theory and accelerated sampling. *arXiv preprint arXiv:2206.07673*, 2022.
- [16] Rossky PJ, Dolly JD, Friedman HL. Brownian Dynamics as Smart Monte Carlo Simulation. *J. CHEM. PHYS.*, USA, vol. 69, no. 10, pp. 4628-4633, 1978.
- [17] Arthur Jacot and Franck Gabriel and Clément Hongler. Neural Tangent Kernel: Convergence and Generalization in Neural Networks. *arXiv preprint arXiv:1806.07572*, 2020.

- [18] G. O. Roberts and A. Gelman and W. R. Gilks. Weak Convergence and Optimal Scaling of Random Walk Metropolis Algorithms. *The Annals of Applied Probability*, vol. 7, no. 1, pages 110–120, 1997.
- [19] Gareth O. Roberts and Jeffrey S. Rosenthal. Optimal Scaling of Discrete Approximations to Langevin Diffusions. *Journal of the Royal Statistical Society. Series B (Statistical Methodology)*, vol. 60, no. 1, pages 255–268, 1998.
- [20] S. L. Cotter and G. O. Roberts and A. M. Stuart and D. White. MCMC Methods for Functions: Modifying Old Algorithms to Make Them Faster. *Statistical Science*, 28(3): <http://dx.doi.org/10.1214/13-sts421>, August 2013.
- [21] Joshua V. Dillon and Ian Langmore and Dustin Tran and Eugene Brevdo and Srinivas Vasudevan and Dave Moore and Brian Patton and Alex Alemi and Matt Hoffman and Rif A. Saurous. TensorFlow Distributions. *arXiv preprint arXiv:1711.10604*, 2017.
- [22] Andrew Gelman and Donald B. Rubin. Inference from Iterative Simulation Using Multiple Sequences. *Statistical Science*, vol. 7, no. 4, pages 457 – 472, 1992, DOI: 10.1214/ss/1177011136.
- [23] Stephen P. Brooks and Andrew Gelman. General Methods for Monitoring Convergence of Iterative Simulations. *Journal of Computational and Graphical Statistics*, vol. 7, no. 4, pages 434–455, 1998.
- [24] Dan Hendrycks and Kevin Gimpel. Gaussian Error Linear Units (GELUs). *arXiv preprint arXiv:1606.08415*, 2023.
- [25] Carl Edward Rasmussen and Christopher K. I. Williams. Gaussian processes for machine learning. MIT Press, 2006, pages I-XVIII, 1-248.

A Proof of Theorem 2.1

Let the assumptions of Theorem 2.1 hold. We start by analysing the general expression of the MCMC acceptance probability:

$$a = \min \left\{ 1, \frac{p(\phi^*|\mathcal{D})q(\phi|\phi^*)}{p(\phi|\mathcal{D})q(\phi^*|\phi)} \right\}.$$

We have already shown that $q(\phi^*|\phi) = \mathcal{N}(\sqrt{1 - \beta^2}\phi, \beta^2 I_D)$. Regarding the reparametrized weight posterior of the network, we observe that [15]

$$\begin{aligned} p(\phi|\mathcal{D}) &= p(\phi^{(L+1)}|\phi^{(\leq L)}, \mathcal{D})p(\phi^{(\leq L)}|\mathcal{D}) \\ &\propto p(\phi^{(L+1)}|\phi^{(\leq L)}, \mathcal{D})\sqrt{\det(\Sigma)}\exp\left(\frac{1}{2}y^T(\sigma^2 I_n + \Psi\Psi^T)^{-1}y\right) \end{aligned}$$

where $p(\phi^{(L+1)}|\phi^{(\leq L)}, \mathcal{D}) \sim \mathcal{N}(0, I_{d^{(L)}})$ is assured by the reparametrisation. It is then crucial to recognize the empirical NNGP kernel $\hat{K}_{\sigma^2} = \sigma^2 I_n + \Psi\Psi^T$ [25] and observe that $\det(\Sigma) \propto \det(\hat{K}_{\sigma^2})$.

Inserting everything in the expression of the acceptance probability we have:

$$\begin{aligned} \frac{p(\phi^*|\mathcal{D})q(\phi|\phi^*)}{p(\phi|\mathcal{D})q(\phi^*|\phi)} &= \frac{p(\phi^{*(\leq L)}|\mathcal{D})p(\phi^{*(L+1)}|\phi^{*(\leq L)}, \mathcal{D})q(\phi|\phi^*)}{p(\phi^{(\leq L)}|\mathcal{D})p(\phi^{(L+1)}|\phi^{(\leq L)}, \mathcal{D})q(\phi^*|\phi)} \\ &= \frac{p(\phi^{*(\leq L)})\sqrt{\det(\Sigma^*)}\exp\left(\frac{1}{2}y^T(\sigma^2 I_n + \Psi^*\Psi^{*T})^{-1}y\right)p(\phi^{*(L+1)}|\phi^{*(\leq L)}, \mathcal{D})q(\phi|\phi^*)}{p(\phi^{(\leq L)})\sqrt{\det(\Sigma)}\exp\left(\frac{1}{2}y^T(\sigma^2 I_n + \Psi\Psi^T)^{-1}y\right)p(\phi^{(L+1)}|\phi^{(\leq L)}, \mathcal{D})q(\phi^*|\phi)} \end{aligned}$$

Where we denote with Σ^* and Ψ^* the covariance matrix and scaled input matrix of the redout layer in equation 3, but for a network with weights ϕ^* . Now:

$$\begin{aligned} q(\phi|\phi^*) &\propto \exp\left(-\frac{1}{2\beta^2}\|\phi - \sqrt{1 - \beta^2}\phi^*\|^2\right) \\ &= \exp\left(-\frac{1}{2\beta^2}\|\phi\|^2 - \frac{(1 - \beta^2)}{2\beta^2}\|\phi^*\|^2 + \frac{\sqrt{1 - \beta^2}}{\beta^2}\phi^T\phi^*\right) \\ &= \exp\left(-\frac{1}{2\beta^2}\|\phi\|^2 - \frac{1}{2\beta^2}\|\phi^*\|^2 + \frac{1}{2}\|\phi^*\|^2 + \frac{\sqrt{1 - \beta^2}}{\beta^2}\phi^T\phi^*\right) \end{aligned}$$

From which

$$\frac{q(\phi|\phi^*)}{q(\phi^*|\phi)} = \exp\left(\frac{1}{2}\|\phi^*\|^2 - \frac{1}{2}\|\phi\|^2\right)$$

and since

$$\begin{aligned} p(\phi^{*(\leq L)})p(\phi^{*(L+1)}|\phi^{*(\leq L)}, \mathcal{D}) &\propto \exp\left(-\frac{1}{2}\|\phi^{*(\leq L)}\|^2\right) \exp\left(-\frac{1}{2}\|\phi^{*(L+1)}\|^2\right) \\ &= \exp\left(-\frac{1}{2}\|\phi^*\|^2\right) \end{aligned}$$

we obtain

$$\begin{aligned} \frac{p(\phi^*|\mathcal{D})q(\phi|\phi^*)}{p(\phi|\mathcal{D})q(\phi^*|\phi)} &= \frac{\exp\left(-\frac{1}{2}\|\phi^*\|^2\right) \exp\left(\frac{1}{2}\|\phi^*\|^2\right) \sqrt{\det(\Sigma^*)} \exp\left(\frac{1}{2}y^T(\sigma^2 I_n + \Psi^* \Psi^{*T})^{-1}y\right)}{\exp\left(-\frac{1}{2}\|\phi\|^2\right) \exp\left(\frac{1}{2}\|\phi\|^2\right) \sqrt{\det(\Sigma)} \exp\left(\frac{1}{2}y^T(\sigma^2 I_n + \Psi \Psi^T)^{-1}y\right)} \\ &= \frac{\sqrt{\det(\Sigma^*)} \exp\left(\frac{1}{2}y^T(\sigma^2 I_n + \Psi^* \Psi^{*T})^{-1}y\right)}{\sqrt{\det(\Sigma)} \exp\left(\frac{1}{2}y^T(\sigma^2 I_n + \Psi \Psi^T)^{-1}y\right)} \\ &\propto \frac{\sqrt{\det(\hat{K}_{\sigma^2}^*)} \exp\left(\frac{1}{2}y^T(\hat{K}_{\sigma^2}^*)^{-1}y\right)}{\sqrt{\det(\hat{K}_{\sigma^2})} \exp\left(\frac{1}{2}y^T(\hat{K}_{\sigma^2})^{-1}y\right)} \end{aligned}$$

To conclude, we exploit the known convergence of the empirical NNGP kernel to a constant independent of $\phi^{\leq L} = \theta^{\leq L}$

$$\hat{K}_{\sigma^2} \rightarrow K_{\sigma^2} \quad \text{as } d_{min} \rightarrow \infty$$

This proves that the numerator and the denominator converge to the same quantity and, consequently, that their ratio converges to 1.

Implying the thesis

$$a = 1 \wedge \frac{p(\phi^*|\mathcal{D})q(\phi|\phi^*)}{p(\phi|\mathcal{D})q(\phi^*|\phi)} \rightarrow 1 \wedge 1 = 1 \quad \text{for } d_{min} \rightarrow \infty$$

B Proof of Theorem 2.2

The proof of Theorem 2.2 relies heavily on results obtained along the proof of Theorem 2.1.

Let's start by writing explicitly the expressions of the acceptance probability for the pCNL algorithm:

$$\begin{aligned} \rho(\phi, \phi^*) - \rho(\phi^*, \phi) &= \\ &= -\ell(\phi) - \frac{1}{2}\langle \phi^* - \phi, \mathcal{D}\ell(\phi) \rangle - \frac{\delta}{4}\langle \phi + \phi^*, \mathcal{D}\ell(\phi) \rangle + \frac{\delta}{4}\|\sqrt{C}\mathcal{D}\ell(\phi)\|^2 \\ &\quad + \ell(\phi^*) + \frac{1}{2}\langle \phi - \phi^*, \mathcal{D}\ell(\phi^*) \rangle + \frac{\delta}{4}\langle \phi + \phi^*, \mathcal{D}\ell(\phi^*) \rangle - \frac{\delta}{4}\|\sqrt{C}\mathcal{D}\ell(\phi^*)\|^2 \\ &= -\ell(\phi) + \ell(\phi^*) - \frac{1}{2}\langle \phi - \phi^*, \mathcal{D}\ell(\phi) + \mathcal{D}\ell(\phi^*) \rangle \\ &\quad - \frac{\delta}{4}\langle \phi + \phi^*, \mathcal{D}\ell(\phi) - \mathcal{D}\ell(\phi^*) \rangle + \frac{\delta}{4}(\|\mathcal{D}\ell(\phi)\|^2 - \|\mathcal{D}\ell(\phi^*)\|^2) \end{aligned}$$

Now, we can exploit previous results to evaluate the likelihood distribution:

$$\begin{aligned} \exp\{\ell(\phi)\} &= \frac{p(\phi|\mathcal{D})p(\mathcal{D})}{p(\phi)} = \\ &= \frac{C_1(\mathcal{D})p(\phi^{(L+1)}|\phi^{(\leq L)}, \mathcal{D})p(\phi^{(\leq L)})\sqrt{\det(\Sigma)} \exp\left(\frac{1}{2}y^T(\sigma^2 I_n + \Psi \Psi^T)^{-1}y\right)}{p(\phi)} \\ &= C_1(\mathcal{D})\sqrt{\det(\Sigma)} \exp\left(\frac{1}{2}y^T(\sigma^2 I_n + \Psi \Psi^T)^{-1}y\right) \end{aligned}$$

where C_1 is a suitable distribution depending only on data. The last equality is due to the fact that $p(\phi^{(L+1)}|\phi^{(\leq L)}, \mathcal{D})p(\phi^{(\leq L)}) \propto \exp(-\frac{1}{2}\|\phi\|^2)$ and the prior $p(\phi)$ is assumed to be a standard Gaussian.

As already done in the proof for pCN sampler we recognize the empirical NNGP kernel \hat{K}_{σ^2} , and we recall that as the minimum layer width goes to ∞ , it converges to a constant independent of the weights K_{σ^2} .

Hence, noting that the Fréchet derivative is a bounded linear operator (thus continuous), by continuous mapping theorem we can conclude that $\mathcal{D}\ell(\phi) \rightarrow 0$ as the layer width goes to ∞ . Since the same goes for $\mathcal{D}\ell(\phi^*)$, we can conclude that in the wide-width limit, all the terms containing Fréchet derivatives of the log-likelihood, evaluated at any point, vanish. As a result, in the wide-width regime, the acceptance rate of the pCNL sampler converges to the one of pCN and, thus, converges to 1.

C Proof of Theorem 3.1

Since we are sampling only from the inner-weights $\theta^{(\leq L)} = W$ of the BNN, the acceptance probability becomes

$$a = 1 \wedge \frac{p(W|\mathcal{D})q(W|W^*)}{p(W|\mathcal{D})q(W^*|W)}$$

By definition 2, $p(W|\mathcal{D}) = p(\phi^{(\leq L)}|\mathcal{D})$ and thus we can exploit the known expressions from Appendix A:

$$\begin{aligned} p(W|\mathcal{D}) &= p(W)\sqrt{\det(\Sigma)}\exp\left(\frac{1}{2}y^T(\sigma^2 I_n + \Psi\Psi^T)^{-1}y\right) \\ &\propto \exp\left(-\frac{1}{2}\|W\|^2\right)\sqrt{\det(\Sigma)}\exp\left(\frac{1}{2}y^T(\sigma^2 I_n + \Psi\Psi^T)^{-1}y\right) \end{aligned}$$

Moreover

$$\begin{aligned} q(W|W^*) &\propto \exp\left(-\frac{1}{2\beta^2}\|W - \sqrt{1-\beta^2}W^*\|^2\right) \\ &\implies \frac{q(W|W^*)}{q(W^*|W)} = \exp\left(\frac{1}{2}\|W^*\|^2 - \frac{1}{2}\|W\|^2\right) \end{aligned}$$

Putting all together and simplifying we get:

$$\begin{aligned} a &= 1 \wedge \frac{\pi(W^*|\mathcal{D})q(W|W^*)}{\pi(W|\mathcal{D})q(W^*|W)} \\ &= 1 \wedge \frac{\sqrt{\det(\Sigma^*)}\exp\left(\frac{1}{2}y^T(\sigma^2 I_n + \Psi^*\Psi^{*T})^{-1}y\right)}{\sqrt{\det(\Sigma)}\exp\left(\frac{1}{2}y^T(\sigma^2 I_n + \Psi\Psi^T)^{-1}y\right)} \end{aligned}$$

That corresponds to the same exact expression found in Appendix A and hence convergence to 1 as the layers width increases is granted by the same arguments.